Mechanism of passive layer formation on AA2024-T3 from alkaline lithium carbonate solutions in the presence of sodium chloride

Visser, Peter; Gonzalez-Garcia, Yaiza; Mol, Johannes M.C.; Terryn, Herman

DOI
10.1149/2.1011802jes

Publication date
2018

Document Version
Final published version

Published in
Journal of the Electrochemical Society

Mechanism of Passive Layer Formation on AA2024-T3 from Alkaline Lithium Carbonate Solutions in the Presence of Sodium Chloride

Peter Visser,[1,2,z] Yaiza Gonzalez-Garcia,[1] Johannes M. C. Mol,[1,*] and Herman Terryn[1,3,*]

[1]*Department of Materials Science and Engineering, Delft University of Technology, 2628 CD Delft, The Netherlands*
[2]*AkzoNobel, 2171 AJ Sassenheim, The Netherlands*
[3]*Research Group of Electrochemistry and Surface Engineering (SURF), Vrije Universiteit Brussel, 1050 Brussels, Belgium*

This study focuses on the elucidation of the formation mechanism of passive layers on AA2024-T3 during the exposure to alkaline lithium carbonate solutions in the presence of sodium chloride. Under controlled conditions, in an electrochemical cell, a protective layer was generated comprising an amorphous inner layer and a crystalline outer-layer. In order to resolve the formation mechanism, the layers were characterized using surface analytical techniques to characterize the surface morphology, thickness and elemental composition of the layers at different stages of the formation process. In addition, electrochemical techniques were applied to link the electrochemical properties of the layers with the different stages of formation. The results demonstrate that the formation mechanism of these layers comprises three different stages: (I) oxide thinning, (II) anodic dissolution and film formation, followed by (III) film growth through a competitive growth-dissolution process. The passive properties of the layers are generated in the third stage through the densification of the amorphous layer. The combined results provide an enhanced insight in the formation mechanism and the development of the passive properties of these layers when lithium salts are used as leaching corrosion inhibitor for coated AA2024-T3.

 [DOI: 10.1149/2.1011802jes]

Manuscript submitted November 7, 2017; revised manuscript received January 15, 2018. Published January 23, 2018.

Lithium salts gained interest as corrosion inhibitor after the observations of unexpected passivity of aluminum in alkaline lithium solutions by Gui and Devine.[1] Aluminum is stable in the range of pH 4 to pH 9 due to the passivity of aluminum oxide.[2] However, it is known that aluminum shows a high corrosion rate at pH values higher than 10.[3] The corrosion process under these alkaline conditions is dominated by two subsequent sub-processes leading to significant mass loss. First, there is the process of direct (anodic) dissolution of the aluminum metal and the formation of an amorphous aluminum hydroxide gel film on the aluminum substrate, and second, the process of chemical dissolution of the aluminum hydroxide gel film into the bulk solution.[4] In contrast, aluminum shows a passive behavior by the formation of a lithium containing film when exposed to alkaline lithium salt solutions.[1,5]

This passive behavior was implemented by Buchheit et al. with the development of a hexavalent chromium-free chemical conversion coating from alkaline lithium carbonate solutions (pH 11–13), generating lithium aluminum carbonate hydroxide hydrate (hydrotalcite) layers on aluminum alloys.[6] They studied the composition, structure and performance of these conversion coatings in relation to processing parameters and various bath chemistries and demonstrated that these hydrotalcite coatings exhibit similar corrosion protective properties as traditional conversion coatings.[7] However, application of these conversion coatings in combination with coatings did not result in an equal performance compared to hexavalent chromium-based conversion coatings.[8]

In 2010, it was discovered that lithium salts could be considered as a potential alternative for chromate-based corrosion inhibitors for the protection of aluminum alloys. Visser and Hayes demonstrated the use of lithium salts as active corrosion inhibitor when incorporated as leachable inhibitor in organic coatings.[9] Further studies have shown the promising corrosion protective performance of this lithium leaching coating technology compared to chromates.[10] Initial observations and characterizations revealed that a film with a three-layered morphology was generated in a defect area.[11–13] This layer was formed under alkaline conditions around pH 10 in the presence of lithium ions, which were leached from the organic coating matrix under corrosive conditions.[14] Electrochemical characterization experiments revealed that the corrosion inhibiting properties of this layer could be attributed to a dense inner layer present at the aluminum metal/oxide interface.[15]

Recently, new examples of the corrosion protective properties of lithium on aluminum were published. Gharbi et al. observed a protective Li/Al surface film on Al-Cu-Li 2050-T3 alloy after polarization.[16] It was postulated that, Li from the substrate stabilized the generated aluminum hydroxide gel film. In addition to this, Mata et al. performed low temperature sealing of tartaric sulfuric acid anodized AA2024-T3 using lithium solutions.[17] Li-Al layered double hydroxide (LDH) structures were formed inside the pores of the anodic aluminum oxide layer by a conversion process providing improved barrier properties and improved stability of the dense oxide layer at the metal/porous oxide interface compared to the conventional hot water sealing treatments.

Our preceding studies of the lithium leaching coatings were focused on the characterization, formation, and electrochemical properties of the protective layers generated in coating defect areas when exposed to accelerated corrosion testing. However, the mechanism and the different steps of formation of such passive layers and the role of lithium under such corrosive conditions have not been studied in detail and need further elucidation.

This work aims to investigate the formation mechanism and the development of the electrochemical properties of these layers on AA2024-T3 by mimicking the aqueous conditions of a defect area in an electrochemical cell filled with a lithium carbonate-NaCl solution. Therefore, a similar layer, as observed in a coating defect when lithium salts are applied as leaching inhibitor, was generated under conversion conditions in an electrochemical cell.[11] The formation of this layer was studied using a combination of surface analytical and electrochemical techniques to gain more understanding about the formation mechanism involved and the development of the corrosion protective properties of the layer during its development under these conditions. The surface morphology was studied with scanning electron microscopy (SEM). The chemical composition and thickness of the layer was monitored with Auger electron spectroscopy (AES) depth-profiles. X-ray photoelectron spectroscopy (XPS) was applied

*Electrochemical Society Member.
[z]E-mail: p.visser-1@tudelft.nl

to detect lithium in the layer. In addition, potentiodynamic polarizations and electrochemical impedance spectroscopy (EIS) were applied to study the electrochemical properties of the generated layer. The study provides an enhanced insight in the formation mechanism of these layers and links the electrochemical properties of the layers with the distinct stages of formation when AA2024-T3 is exposed to alkaline lithium carbonate-NaCl solutions.

Experimental

Materials and sample preparation.—Unpolished samples of AA2024-T3 (5.0 × 7.0 cm, 0.8 mm thickness) were used as supplied. In order to generate an equal and reproducible starting point for all samples, the substrates were pretreated as follows. The panels were degreased with acetone to remove surface contaminations. This was followed by an immersion in a commercial alkaline cleaning solution (Ridoline 1402) for 1 minute at 55–60°C. After a rinse in deionized water the panels were subjected to a deoxidation step in a 1 M nitric acid solution for 4 minutes at 20–25°C, followed by a rinse in deionized water. Finally the panels were dried under ambient conditions.

Electrolyte compositions.—The composition of electrolyte used in this work is based on three factors: 1) an estimated Li-concentration in a defect area when leaching from a coating, calculated from the coating thickness, lithium carbonate loading, volume of defect area and the lithium depletion depth into the coating; 2) the moderate alkaline pH as measured in a coating defect(14); 3) the thickness and morphology of the layer generated in a coating defect after 4 hours exposure to neutral salt spray conditions (ASTM B-117).[11]

Lithium carbonate (Li_2CO_3) was acquired form Sigma-Aldrich and the Li_2CO_3-NaCl solution was prepared by mixing 0.01M Li_2CO_3 into a 5% NaCl solution. The pH was measured prior to each experiment in general the pH of this solution was between 10.5 and 10.7. The solution will be referred to as the Li_2CO_3-NaCl solution throughout the manuscript.

Formation of the passive layers in an electrochemical cell.—The panels were placed as a working electrode in an electrochemical cell set-up (exposed area of 12.7 cm^2) using an Ag/AgCl reference electrode and a platinum gauze counter electrode. The panels were exposed to 5 ml of the Li_2CO_3-NaCl solution (pH = 10.5 – 10.7). The aluminum samples were exposed under aerated conditions from 80 s up to 4 h. During the exposure to the Li_2CO_3-NaCl solution the open circuit potential was monitored to study the formation of the passive layer and ensure the reproducibility of the process. After the specific time of exposure to the Li_2CO_3-NaCl solution, the samples were rinsed directly with copious amounts deionized water prepared with a Millipore system to quench the formation process.

Reference samples for surface analysis.—Reference samples of pseudoboehmite (PB) and Li-layered double hydroxide (Li-LDH) on AA2024-T3 aluminum alloy were prepared for comparison purposes in the X-ray photoelectron spectroscopy section. Pseudoboehmite was prepared by treating the panel with deionized water at 95–100° C for 1h according to the method of Gorman et al.[18] The Li-LDH reference was prepared by immersing a AA2024-T3 panel in a 0.1 M Li_2CO_3 solution (pH = 11.3) for 15 min using the conversion coating process of Buchheit et al.[6] Following the treatment, the panels were rinsed with deionized water for 5 min and dried at the air.

Surface analytical measurements.—*Scanning electron microscopy (SEM).*—The surface morphology of the layers was examined using a JEOL JSM-7100F Field-Emission SEM (FESEM) microscope using the secondary electron detector (SEI) at a working distance of 10 mm and an acceleration voltage of 5 kV. The cross-section of the layer after 4 hours exposure to the Li_2CO_3-NaCl solution was examined in a ZEISS Ultra 55 microscope at a 0.5 kV acceleration voltage. The cross-sections of the aluminum panels were prepared with a Leica EM UC6 ultra-microtome equipped with a diamond knife.

Auger electron spectroscopy (AES).—Elemental depth profiles were acquired using a PHI 650(SAM) with a LaB6 cathode and a Cylindrical Mirror Analyzer (CMA). The samples were analyzed with a surface incident angle of 30° to the normal using a primary electron beam with an energy of 5 keV and an emission current of 1 μA, with a base pressure of 3 × 10^{-10} Torr in the analysis chamber. A PHI 04–303 ion gun and 3 keV Ar ions (emission current of 20 mA and Ar pressure of 10 mPa) was used for ion sputtering (1 mm^2 raster). The sample surface was impinged with the ion-beam angle of 50° to the normal using 1 minute intervals. Multipak (V8.0) software was used to analyze the recorded spectra.

X-ray photoelectron spectroscopy (XPS).—A PHI 1600/3057 instrument was used to study the surface chemistry of the samples using an incident X-ray radiation (Mg Kα1,2 = 1253.6 eV). All the measurements were performed with a takeoff angle of 45° with respect to the sample surface and an analysis chamber base vacuum of about 5 × 10^{-9} Torr. High resolution scans of the Li1s, Mg1s, Cu2p, O1s, Al2p and C1s photo peaks were recorded without the use of a neutralizer from a 400 μm sample spot diameter, applying a pass-energy of 23.5 eV and 0.1 eV step size. The recorded spectra were calibrated relative to the C1s peak at a binding energy of 284.8 eV to correct for sample charging. The evaluation of the spectra was carried out using the PHI Multipak V9.5.0.8. software. Curve fitting was performed according to the method of Abrahami et al. using a Shirley-type background removal and mixed Gaussian Lorentzian shapes (80–100%).[19] The depth profile was prepared with Ar- ion sputtering using a PHI 04–303 ion gun and 3 keV Ar ions (emission current of 20 mA and Ar pressure of 10 mPa). The surface was rastered over an area of 2 mm^2. The ion beam was used at intervals of 1 minute and impinged on the sample surface at 50° to the normal.

Electrochemical measurements.—The electrochemical measurements were conducted in a conventional three-electrode cell using an Autolab PGSTAT 30 potentiostat and Nova data collection Software (version 1.10). The reference electrode was a saturated Ag/AgCl electrode, platinum gauze was utilized as counter electrode, and the aluminum sample was used as the working electrode. All measurements were conducted in a Faraday cage.

Open Circuit Potential measurements (OCP) were performed during the exposure to the Li_2CO_3-NaCl solution (exposed area 12.7 cm^2), to study the electrochemical response of the substrate during the deposition of the passive layer in-situ and as a function of time.

Potentiodynamic polarizations were performed according to ASTM G57-97 using a sweep range of −200 to +200 mV versus the OCP at a sweep rate of 0.1667 mV/s on a surface area of 0.50 cm^2 after an OCP stabilization period of 2 h in a 0.05 M NaCl solution. Different samples were used for each anodic or cathodic polarization. At least two separate anodic and cathodic polarizations were performed for each sample to ensure reproducibility.

Electrochemical Impedance Spectroscopy (EIS) measurements were conducted at the OCP in the frequency range of 10^5 Hz to 10^{-2} Hz with 10 points per decade and a sinusoidal potential perturbation of ±10 mV. The exposed area of the samples was 3.14 cm^2 using 60 ml of 0.05 M NaCl electrolyte. Measurements were performed after 4 h exposure to the 0.05 M NaCl electrolyte on at least three samples for each stage of formation. The impedance plots were fitted with Zview from Scribner Associates Inc., using the appropriate equivalent circuits.

Results and Discussion

Generation of the passive layer in an electrochemical cell.—The first objective of this study was to generate a similar layer as observed in a coating defect under conversion conditions in an electrochemical

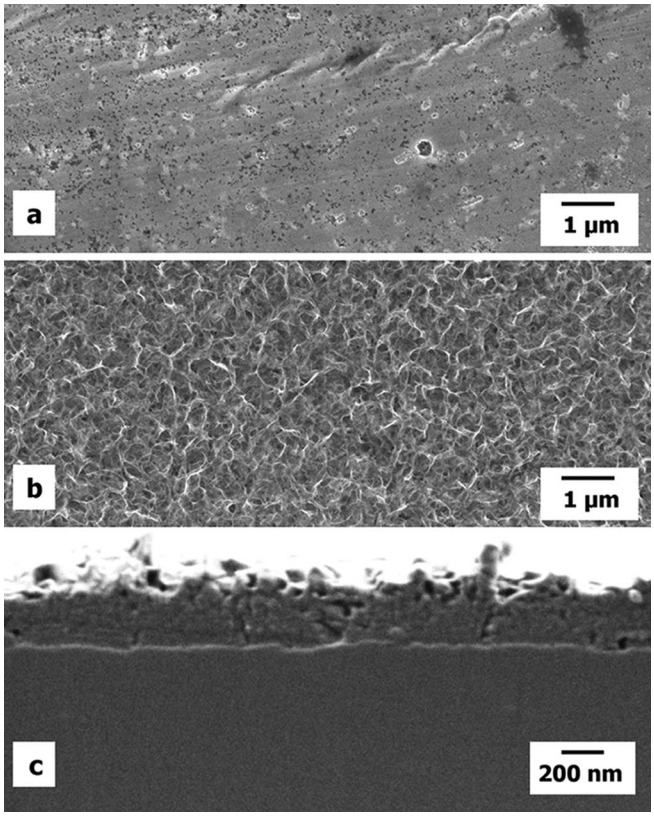

Figure 1. Scanning electron micrographs of AA2024-T3 surface (a) prior to exposure; (b) after 4 h exposure; (c) cross-section of the layer after 4 h exposure to the Li_2CO_3-NaCl solution.

cell. The formation process by leaching from a coating can differ significantly from the "static" conversion process in the electrochemical cell in terms of lithium concentration gradients and the thin film formation processes. For this part of the work, an AA2024-T3 surface was exposed to the Li_2CO_3-NaCl solution for 4 hours. Fig. 1 shows scanning electron micrographs of the surface of AA2024-T3 aluminum prior and after exposure to the Li_2CO_3-NaCl solution. Fig. 1a shows the AA2024-T3 substrate surface after alkaline cleaning and the deoxidation steps prior to exposure and Fig. 1b shows the aluminum surface with the formed layer after 4 h exposure to the Li_2CO_3-NaCl solution. Fig. 1c shows the cross-sectional micrograph of this layer observed in Fig. 1b. The generated layer is about 300 to 400 nm thick and shows a dense morphology at the aluminum metal/oxide interface (inner layer) and a porous morphology at the outer layer. The layer is similar in terms of thickness and morphology compared to the layer formed in a defect area after 4 h neutral salt spray exposure, when lithium carbonate was used as leachable corrosion inhibitor in organic coatings.[11] This demonstrates that similar layers could be generated in an electrochemical cell from lithium carbonate solutions with a moderate pH and in the presence of NaCl.

Open circuit potential during the formation of the layer.—The 0.01M Li_2CO_3-NaCl solution was used to study the formation of the layer as a function of time using an OCP in-situ measurement to identify the different stages of the formation. Fig. 2 shows the OCP evolution of the AA2024-T3 aluminum alloy measured during the formation of the layer when it is exposed to the Li_2CO_3-NaCl solution for 4 h. From the OCP evolution, three stages can be identified. Stage 1 (Fig. 2 inset) is the initial rapid potential decrease to a minimum of -1.32 $V_{(Ag/AgCl)}$ after 60–80 s of exposure to the Li_2CO_3-NaCl solution. Stage II shows the first potential increase to a plateau of -1.20 $V_{(Ag/AgCl)}$ after 1000 s, and Stage III represents the second potential

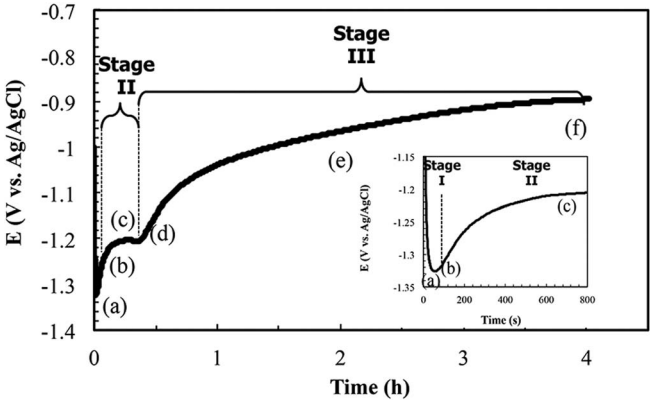

Figure 2. Open circuit potential response over time of AA2024-T3 exposed to the Li_2CO_3-NaCl solution (pH = 10.6): (a) 80 s; (b) 150 s; (c) 700 s; (d) 1400 s; (e) 2 h; (f) 4 h; inset: open circuit response over the first 300 s.

increase toward a plateau of $-0.90V_{(Ag/AgCl)}$ after 4 h. This suggests that the formation of the layer involves multiple sub-processes.

The initial drop of the potential, observed in Stage I, can be related to the activation of the aluminum by the exposure to the Li_2CO_3-NaCl solution because aluminum oxide is not stable at pH values higher than 9.[2] In addition to the alkaline conditions, chloride-ions can contribute to the thinning and dissolution of the native aluminum oxide.[20] The thinning of the oxide layer enables electron tunneling and metal ion-migration initiating the anodic dissolution of the substrate.[21] Stage II starts after about 80 s of exposure to the Li_2CO_3-NaCl solution. At this stage, the potential starts to increase rapidly and hydrogen evolution is observed due to the water reduction reaction triggered by the cathodic over-potential.[3] This increase of potential toward the first plateau region can be attributed to the initial formation of the layer due to the anodic dissolution of substrate.[22] The first plateau can be attributed to the lateral coverage of the aluminum substrate with this layer.[22] Stage III shows the second increase of potential indicates the further growth of the layer. It is known that oxide layers grow in thickness over the general aluminum substrate as a result of the cathodic reactions at the oxide surface via electron tunneling through the growing oxide layer or residual flaws in the layer.[23] When the thickness of the layer increases, these cathodic processes decrease and become insignificant resulting in a slow potential increase.[23] This gradual increase, observed between 2 and 4 h suggests a slow but continuous development and densification of the layer on the substrate.

Characterization of the layer during the formation.—In order to study the composition and thickness of this formed layer as function of this OCP behavior, samples haven been taken at the specific time intervals of the formation for further characterization (Fig. 2): Stage I: (a) 80 s, at the OCP minimum; Stage II: (b) 150 s, during the first OCP increase, (c) 700 s, at the first plateau; Stage III: (d) 1400 s, at the second OCP increase, (e) 2 h, second plateau phase, and (f) 4 h, at the end of the process.

Evolution of the surface layer morphology during the formation.— Fig. 3 shows top-view FESEM micrographs of the aluminum alloy surface after the selected periods of exposure to the Li_2CO_3-NaCl solution. Fig. 3a (80 s) shows the surface of the aluminum alloy with the thinned oxide at the minimum of the OCP (stage I). After 150 s (Fig. 3b), the substrate shows the aluminum with a porous morphology indicating initial anodic dissolution of aluminum from the matrix. The micrograph recorded at the OCP plateau in stage II after 700 s (Fig. 3c) clearly shows that the pits and porous nature of the surface observed after 150 s have been covered with small crystals. This indicates that the layer started to form on the aluminum surface. A more pronounced layer is visible after 1400 s exposure to the Li_2CO_3-NaCl solution

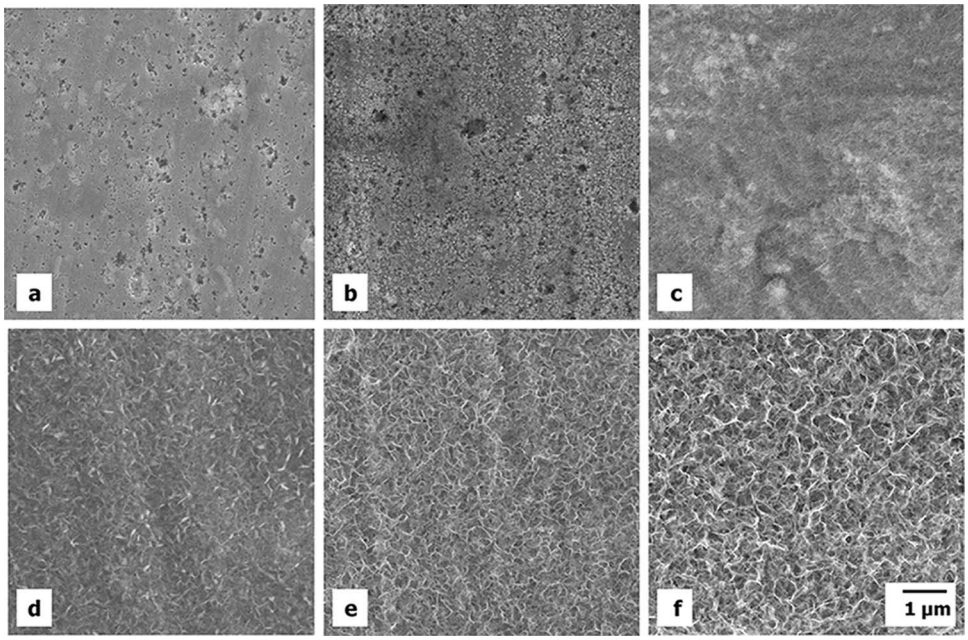

Figure 3. Scanning electron micrographs of AA2024-T3 surface as function of the exposure time to the Li_2CO_3-NaCl solution: (a) 80 s; (b) 150 s; (c) 700 s; (d) 1400 s; (e) 2 h; (f) 4 h.

(Fig. 3d). The crystals have grown and the layer appears to be thicker. Prolonged exposures to this solution of 2 and 4 h (Figs. 3e and 3f) showed the further growth of the layer and the crystals developed into a porous outer layer.

Thickness development of the layer.—Auger depth-profiles were recorded to follow the growth and the elemental composition of layer during the formation on the AA2024-T3 alloy. The KLL lines of oxygen (O) aluminum (Al), magnesium (Mg), copper (Cu), and carbon (C) were recorded. Lithium (Li) could not be detected due to overlap with the aluminum oxide LVV region. The Al KLL peak could be fitted to distinguish between the contribution related to the oxide ($Al_{(oxide)}$) and the substrate ($Al_{(metal)}$).[14] Figs. 4a–4g shows the Auger depth profiles for the samples after the different periods of exposure to the Li_2CO_3-NaCl solution. The thickness of the generated layer can be related to the sputtering time needed to reach the aluminum metal/oxide interface ($t_{sputter\text{-}interface}$). This can be determined by the sputtering time corresponding to an increase of the peak-to-peak intensity of $Al_{(metal)}$ to 50% of its maximum intensity.[24] Fig. 4h summarizes the $t_{sputter\text{-}interface}$ in a graph demonstrating increase of the $t_{sputter\text{-}interface}$ as function of the exposure time to the Li_2CO_3-NaCl solution. From this graph, it can be noticed that $t_{sputter\text{-}interface}$ increased as a result of longer exposure to the Li_2CO_3-NaCl solution. The inset of Fig. 4h shows the early stages of exposure to the solution. Initially, the sample shows a shorter sputtering time compared to the pretreated sample after 80 s and up to 150 s exposure to the Li_2CO_3-NaCl solution there was no significant increase in sputtering time observed. The $t_{sputter\text{-}interface}$ increased rapidly between 150 s and 1400 s exposure to the Li_2CO_3-NaCl solution. This suggests that the initial growth of the layer occurs in this period of time. The increase of $t_{sputter\text{-}interface}$ reduced when the samples were exposed to the Li_2CO_3-NaCl solution beyond 1400 s, up to 4 h, suggesting a slower growth rate of the layer compared to the initial growth between 150 and 1400 s exposure to the solution.

In terms of composition, the surface oxide is observed by the presence of O and $Al_{(oxide)}$. In the early stages of exposure (up to 150 s) to the Li_2CO_3-NaCl solution the outer oxide layer shows enrichment of Mg. This Mg most likely originates from the S-phase intermetallic particles in the aluminum alloy and is released into the oxide layer by anodic dissolution.[25] The sputter profiles of 700 s and beyond clearly show the presence of a layer consisting mainly of O and $Al_{(oxide)}$. Characteristic for these prolonged exposure times to the Li_2CO_3-NaCl solution is the higher levels of Mg at the Al metal/oxide interface. The presence of Mg and the low levels of Cu suggest that the substrate dissolution during the formation of the layer was limited. Furthermore, the growth rates of the layer reduced after 1400 s exposure to the Li_2CO_3-NaCl solution (Figs. 4f, 4g). In addition to this, the O/Al ratio close to the aluminum metal/oxide interface has increased compared to the O/Al ratio of the outer layer. This could indicate that the composition of the layer close to the aluminum metal/oxide interface is different compared to the outer layer.

The evolution of the sputtering times of the Auger depth-profiles is in line with the 3 phases in the OCP evolution and FESEM observations, showing the oxide thinning after 80 s (Stage I), the growth of the layer between 150 and 1400 s (Stage II) and a gradual growth upon prolonged exposure up to 4 h to the Li_2CO_3-NaCl solution (Stage III).

Elemental composition of the layer during formation.—XPS was applied to study the chemical composition of the layers during the formation process. Table I shows the elemental composition and the O/Al ratio at the different stages of the formation and Table II summarizes the photo peak envelope positions of O1s, $Al2p_{(oxide)}$, $Al2p_{(metal)}$ and Li1s and the full width half-maximum (FWHM) of the peak intensities of O1s and $Al2p_{(oxide)}$. The oxide generated on AA2024-T3 after the pretreatment, consists of O and Al with traces of Mg, Cu and C. At this stage, only oxide related aluminum $Al2p_{(oxide)}$ peak at 74 eV was observed. However, exposure for 80 s to the Li_2CO_3-NaCl solution results in the appearance of the $Al2p_{(metal)}$ peak around 71.4 eV next to the $Al2p_{(oxide)}$, this indicates that the oxide became thinner. In addition to this, the surface area showed an enrichment of Mg (8.1 at. %) and Cu (0.8 at. %) after 150 s which could indicate anodic dissolution of the S-phase intermetallic particles.[25] After 700 s exposure to the Li_2CO_3-NaCl solution, Mg and Cu concentrations decreased and the $Al2p_{(metal)}$ peak disappeared. At this stage, the surface of the layer predominantly consists of Al and O with an O/Al-ratio around 3 and no lithium was detected. After 1400 s, the first significant amount of lithium (1.1 at%) was detected at the surface of the layer and the Mg and Cu concentrations decreased further. The lithium concentration of the surface layer increased to 6.0 at% after respectively 2 and 4 h. Fig. 5 shows the correlation between the lithium concentration

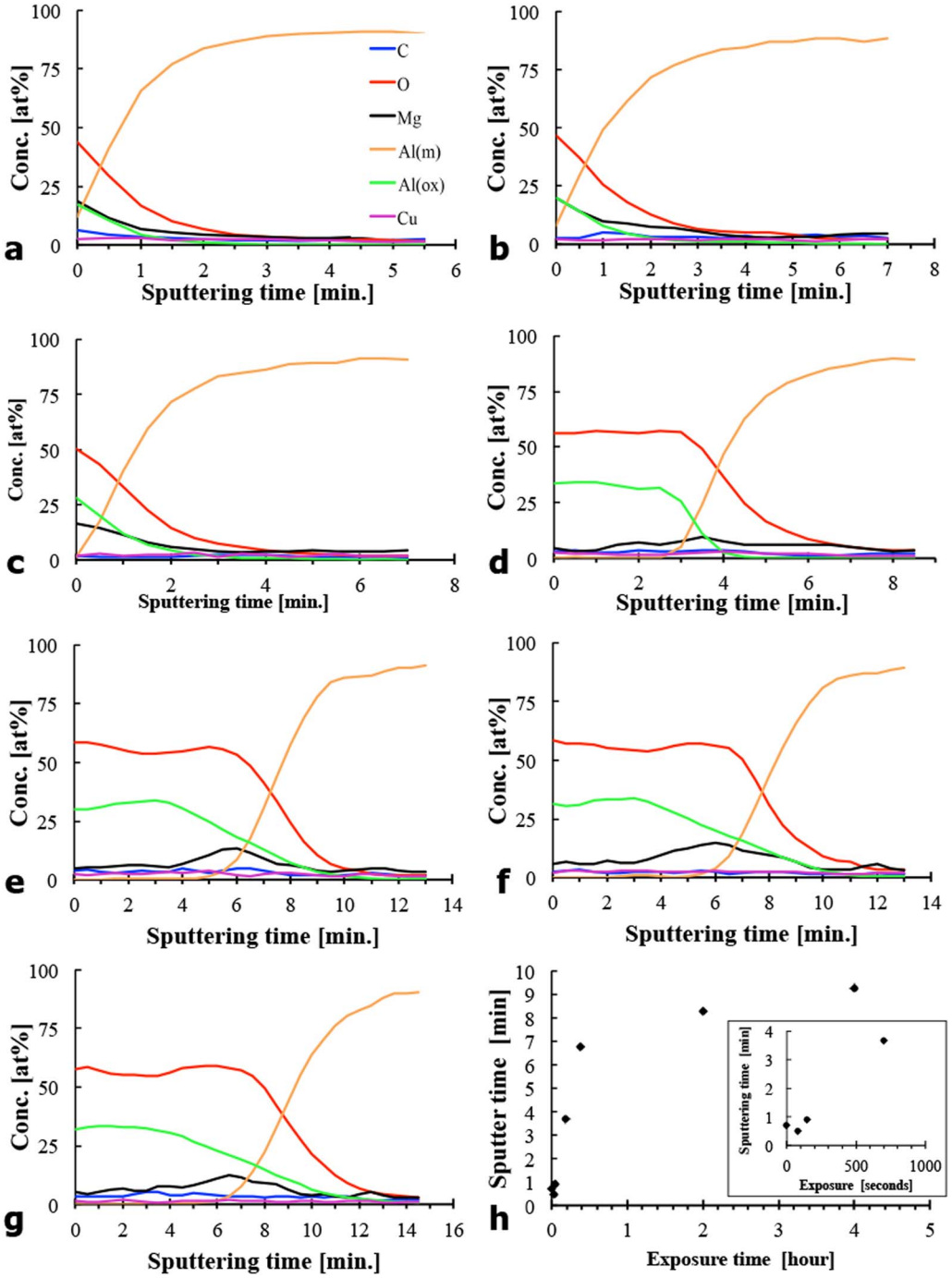

Figure 4. AES depth profiles of the layers formed on AA2024-T3 after exposure to the Li_2CO_3-NaCl solution as function of time: (a) before exposure; (b) 80 s; (c) 150 s; (d) 700 s; (e) 1400 s; (f) 2 h; (g) 4 h; (h) development of sputtering time as function of time of exposure to the Li_2CO_3-NaCl solution.

at the surface of the layer and the increase of the oxide layer thickness represented by the sputtering time to the Al metal/oxide interface ($t_{sputter\text{-}interface}$) in relation the three stages of formation. This figure suggests that the lithium intercalation is related to Stage III of the layer formation.

From Table II, it can be noted that the FWHM of the O1s peak decreases during the formation of the layer from around 3 eV in the early stages to 1.8 eV after 4h exposure to the Li_2CO_3-NaCl solution. The FWHM of the O1s peak relates to the degree of oxide hydration because OH^- and H_2O have a higher binding-energy compared to O^{2-} bond as found in Al-O-Al bonds.[19,26] A three-component deconvolution fitting method of the O1s peak can be applied to determine the relative ratio of the contributions of O^{2-}, OH^- and H_2O in the layer.[19,27] Figure 6 shows selected O1s peaks and examples of the deconvolution before and after the exposure to the Li_2CO_3-NaCl solution. The deconvolution results of all the samples (ratio H_2O / OH^- / O_2^-) are displayed in Table II. Fig. 6a shows the deconvolution of the O1s peak of the oxide layer after the pretreatment but prior to exposure to the Li_2CO_3-NaCl solution. The oxide layer contains a relative small about of H_2O and the majority of the O1s peak can be attributed to OH^- and O_2^-. After the period of oxide thinning (150 s) the FWHM of the O1s peak increased slightly from 2.8 to 3.0 eV. This widening of the O1s peak can be related to the increased contribution of H_2O and O_2^- in the layer (Fig. 6b). The FWHM of the O1s peak

Table I. Elemental composition of the specimen surface at the different exposure times to the Li_2CO_3-NaCl solution measured by XPS.

	Atomic concentration (%)						ratio
	Li 1s	C 1s	O 1s	Mg 1S	Al 2p	Cu 2p	O/Al
initial	0.0	2.8	71.9	6.0	22.6	0.1	3.2
80 s	0.0	2.2	69.9	6.9	20.8	0.4	3.4
150 s	0.0	1.7	67.3	8.1	22.6	0.8	3.0
700 s	0.0	1.3	74.6	1.8	21.8	0.4	3.4
1400 s	1.1	2.5	70.5	0.7	25.1	0.1	2.8
2 h	6.1	4.2	69.9	1.4	18.4	0.1	3.8
4 h	6.5	3.7	69.5	0.8	19.5	0.1	3.6
Reference samples							
pseudoboehmite	-	8	64.5	0.2	27.2	0.1	2.4
Li-LDH	6.6	4.4	69.4	-	19	-	3.7

decreased significantly from 3.0 to approximately 2.0 eV after 700 s exposure to the Li_2CO_3-NaCl solution. Deconvolution of the narrowed O1s peak showed decreased contributions of H_2O and O_2^- and an increased contribution of OH^- (Fig. 6c). Extended exposure to the Li_2CO_3-NaCl solution for 4 h (Fig. 6d) resulted in a further narrowing of the O1s peak to 1.8 eV and fitting revealed a further increase in the contribution of OH^-. The combination of these observations with the data of the elemental composition and reference samples (Tables I and II), indicates that between 150 and 1400 s the surface oxide transformed into $Al(OH)_3$ during the layer growth process. After 150 s, this layer seems to be rather hydrated but the surface layer seems to crystallize upon longer exposure 700–1400 s. Prolonged exposure (2 and 4 h) to the Li_2CO_3-NaCl solution lead to a second transformation of the surface. From the comparison with the reference samples it can be concluded that surface of the layer transformed into a lithium layered double hydroxide (Li-LDH).

Lithium distribution in the layer.—The XPS-analysis demonstrated that the generated layer contains Li-LDH ($Li_2[Al_2(OH)_6]_2 \cdot CO_3 \cdot nH_2O$). Microscopic analysis of the surface of the layer showed the crystalline nature of a Li-LDH (Fig 1b). However, the cross-section (Fig. 1c) and analysis of previous work indicate an amorphous layer below the crystalline top layer.[12] XPS-depth profiling was applied to obtain more detailed information of the elemental composition as a function of depth of the formed layer with a special focus on the lithium concentration. Fig. 7a shows the XPS-depth profile of a generated layer after 4 h exposure to the Li_2CO_3-NaCl solution. Fig. 7b shows the profile for the low concentration elements (Li, C, Cu and Mg). From the profiles it is apparent that the highest concentration of lithium is located at the outer surface of the generated layer. The concentration of lithium decreased rapidly after the first sputtering cycles. After 5 minutes

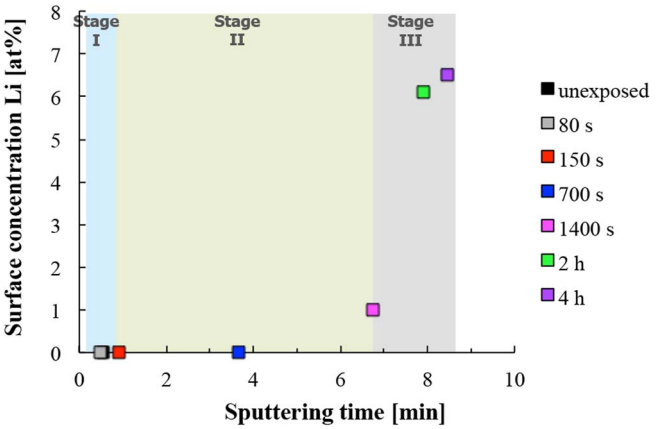

Figure 5. The lithium concentration at the surface of the layer determined by XPS versus the oxide thickness indicated by AES sputtering time to the aluminum metal/oxide interface ($t_{sputter\text{-}interface}$) as a function of exposure time to the Li_2CO_3-NaCl solution, demonstrating the relation of layer growth and lithium intercalation during the three stages of formation.

sputtering the concentration of lithium decreased below 1.0 at% and could not be detected anymore. The sputter profile also shows carbon (C) enrichment of around 2.8 at% at the outer surface of the layer. Upon sputtering, the concentration of the carbon decreased at a similar rate as the lithium concentration. Therefore, this carbon, observed at 289eV, can be attributed to the carbon of the carbonate of Li-LDH. The rest of the layer consists of oxygen (O) and aluminum (Al) and traces of copper (Cu) and magnesium (Mg). Fig. 7b shows as well the enriched Mg concentration at the metal/oxide interface possibly due to anodic dissolution of S-phase intermetallic particles that are present in the alloy.[25] Under these alkaline conditions Mg will precipitate as $Mg(OH)_2$. In addition only traces of Cu dissolved from the alloy. This indicates that there was only limited substrate dissolution during the formation of the layer. These results suggest that only the outer part of the layer is a Li-LDH and the inner layer an aluminum oxide/hydroxide.

Mechanism of formation.—The results of this investigation show that the mechanism of the formation of these layers involves multiple stages. Fig. 8 shows a schematic illustration of these formation stages related to the OCP evolution. First, there is the activation phase (stage I). Aluminum oxide is stable in the pH range from 4 to 9,[28] but the oxide is weakened by adsorption of chloride ions and the alkaline nature (pH 10.6) of the lithium carbonate solution.[20,29] The oxide will be thinned due to the dissolution reaction of the oxide in the alkaline solution (Eq. 1).

$$Al_2O_3 + 2OH^- + 3H_2O \rightleftharpoons 2Al(OH)_4^- \quad [1]$$

Table II. XPS peak positions and the measured FWHM (O and Al) of the specimen surface at the different exposure times to the Li_2CO_3-NaCl solution.

	O1s		Al 2p (oxide)		Al $2p_{(metal)}$	Li 1s	Fitting O1s Rel. ratio
Exposure (time)	BE (eV)	FHWM (eV)	BE (eV)	FHWM (eV)	BE (eV)	Be (eV)	area H_2O / OH^- / O^{2-}
Initial	531.7	2.8	74	1.6	-	-	0.12/ 0.52/ 0.36
80 s	531.5	2.9	74.2	1.8	71.4	-	0.14/ 0.46/ 0.40
150 s	531.3	3	73.9	2.0	71.2	-	0.19/ 0.43/ 0.38
700 s	531.8	2.1	74.3	1.9	-	-	0.05/ 0.71/ 0.24
1400 s	531.5	2.3	74	1.7	-	54.6	0.09/ 0.64/ 0.27
2 h	531.8	1.8	74.4	1.5	-	55.5	0.01/ 0.87/ 0.12
4 h	531.6	1.8	74.1	1.4	-	55.3	0.02/ 0.85/ 0.13
Reference samples							
pseudoboehmite	531.3	2.9	73.8	1.8	-	-	0.03/ 0.44/ 0.53
Li-LDH	531.8	2.0	74.4	1.7	-	55.4	0.02/ 0.95/ 0.03

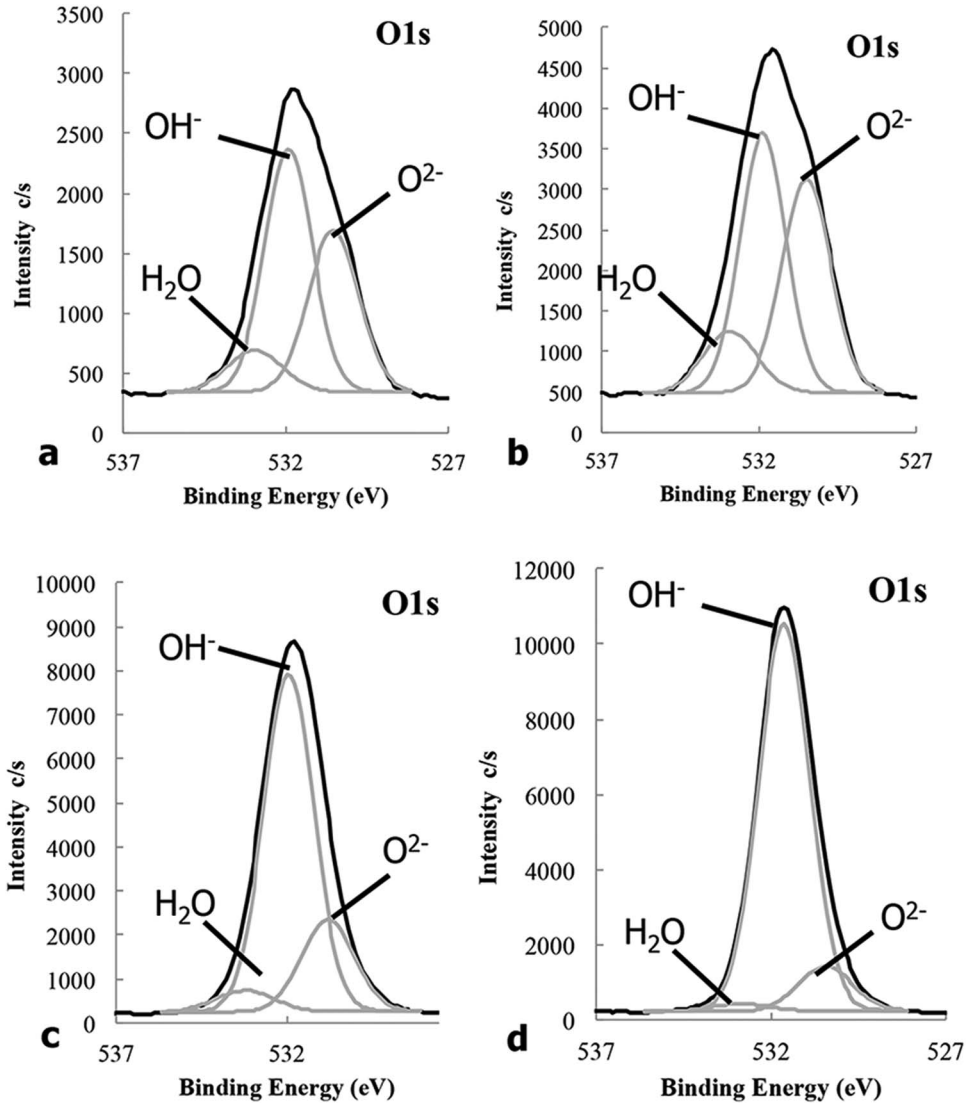

Figure 6. Curve fitting results of high-resolution O1s photo peaks of (a) before; after (b) 150 s, (c) 700 s, and (d) 4 h exposure Li_2CO_3-NaCl solution.

When the oxide is sufficiently thinned, the OCP reaches its minimum value and stage II initiates with the direct (anodic) dissolution of aluminum (Eq. 2). This dissolution results in the formation of an aluminum hydroxide gel layer at the aluminum metal surface (Eq. 3) because aluminum ions are not stable under alkaline conditions.[4,30]

$$Al + 3e^- \rightleftharpoons Al^{3+} \quad [2]$$

$$Al^{3+} + 3OH^- \rightleftharpoons Al(OH)_3 \quad [3]$$

Under these alkaline conditions, the aluminum hydroxide layer will be chemically dissolved at the aluminum hydroxide/solution interface (Eq. 4).[3,4]

$$Al(OH)_3 + OH^- \rightleftharpoons Al(OH)_4^- \quad [4]$$

The rate of dissolution depends on the pH of the environment.[31] Moderate pH values lead to thicker aluminum hydroxide gel layers due to lower dissolution rate compared to the case of high pH conditions. The dissolution of the aluminum hydroxide layer will consequently trigger further anodic dissolution of the aluminum metal resulting in a competitive growth/dissolution reaction. The direct aluminum dissolution is accompanied by hydrogen evolution due to the water reduction reaction (Eq. 5).[4]

$$2e^- + 2H_2O \rightleftharpoons H_2 + 2OH^- \quad [5]$$

During stage II, the open circuit potential increases with time. This can be attributed to the growth of the aluminum hydroxide gel film as observed in the Auger depth profiles recorded after 150 and 1400s exposure to the Li_2CO_3-NaCl solution. The direct dissolution of Al and the growth of the hydroxide layer are suppressed when the layer becomes thicker during stage II. This relation of OCP development and layer growth of aluminum under alkaline conditions has been observed and described earlier by Burstein et al.[32] and Zang et al.[33]

From the surface analysis it seems that lithium does not play an active role in this initial process because no detectable amounts of lithium were observed in the layer during these stages of formation. A slower growth process (Stage III) follows the fast process in Stages I and II.

This third stage is characterized by the competitive growth and dissolution process and intercalation of lithium into the outer layer. Lithium is known for its facile intercalation with aluminum hydroxides to form a layered double hydroxide under alkaline conditions.[34] Li-ions react with the $Al(OH)_4^-$ and the carbonate-ion to form a lithium aluminum hydroxide carbonate hydrate or layered double hydroxide ($Li_2[Al_2(OH)_6]_2.CO_3.nH_2O$ (Li-Al LDH)). Prolonged

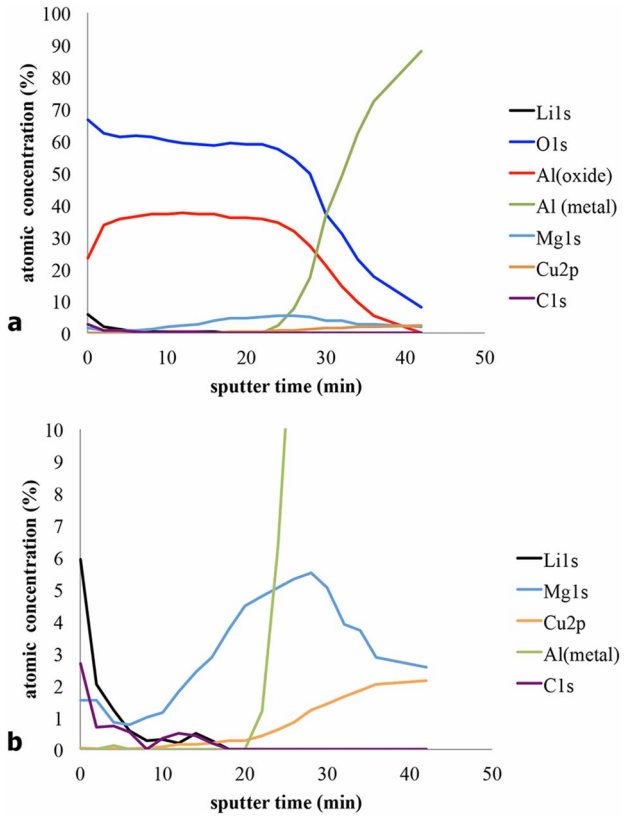

Figure 7. XPS depth-profile of the passive layer formed after 4h exposure to the Li_2CO_3-NaCl solution: (a) complete profile; (b) low concentration elements.

exposure under these conditions resulted in the further growth of the film, thus an increase of the OCP. The competitive growth/dissolution process will proceed until the layer becomes of considerable thickness, limiting the diffusion of OH^- and Al^{3+} ions through the layer or when the pH drops to lower values (<pH 9). From this process it can be postulated that the Li-Al LDH is a side-product resulting from the aging process at the outer layer of the aluminum hydroxide gel under these alkaline conditions in the presence of lithium.

These observations show the three stages involved in the mechanism of formation of a protective layer on AA2024-T3 and provide more insight on the active protective inhibition mechanism of the lithium-leaching coating technology.[14]

Corrosion protective properties during formation of the oxide layer.—*Potentiodynamic polarization measurements.*—Potentiodynamic polarization measurements were performed in a 0.05 M NaCl solution after the same time intervals of exposure to the Li_2CO_3-NaCl solution as studied in the section above (Fig. 9). The polarizations were performed from −0.2 V to 0.2 V vs the open circuit potential. The cathodic branch of the unexposed sample shows a diffusion–limited behavior from potentials lower than 0.54 $V_{(Ag/AgCl)}$. On the other hand the anodic branch of this sample shows no passive region but immediate pitting under potentiodynamic polarization. Exposure to the Li_2CO_3-NaCl solution up to 150 s resulted in an increase of the cathodic current density while the behavior of the anodic polarization remained similar. Exposure to the Li_2CO_3-NaCl solution longer than 700 s resulted in the decrease of the cathodic current density by an order of magnitude. At the same time, the anodic polarization curves show a decrease in the anodic current density and the pitting potential is shifted to more noble potentials. From the graph it can be noted that i_{corr} decreased over time with the decrease of i_{anodic} and $i_{cathodic}$ while the corrosion potential (E_{corr}) remains similar over time. Table III lists the corrosion potential (E_{corr}), the corrosion current densities (i_{corr}), the polarization resistance (R_{pol}) and the pitting potential (E_{pit}) of the

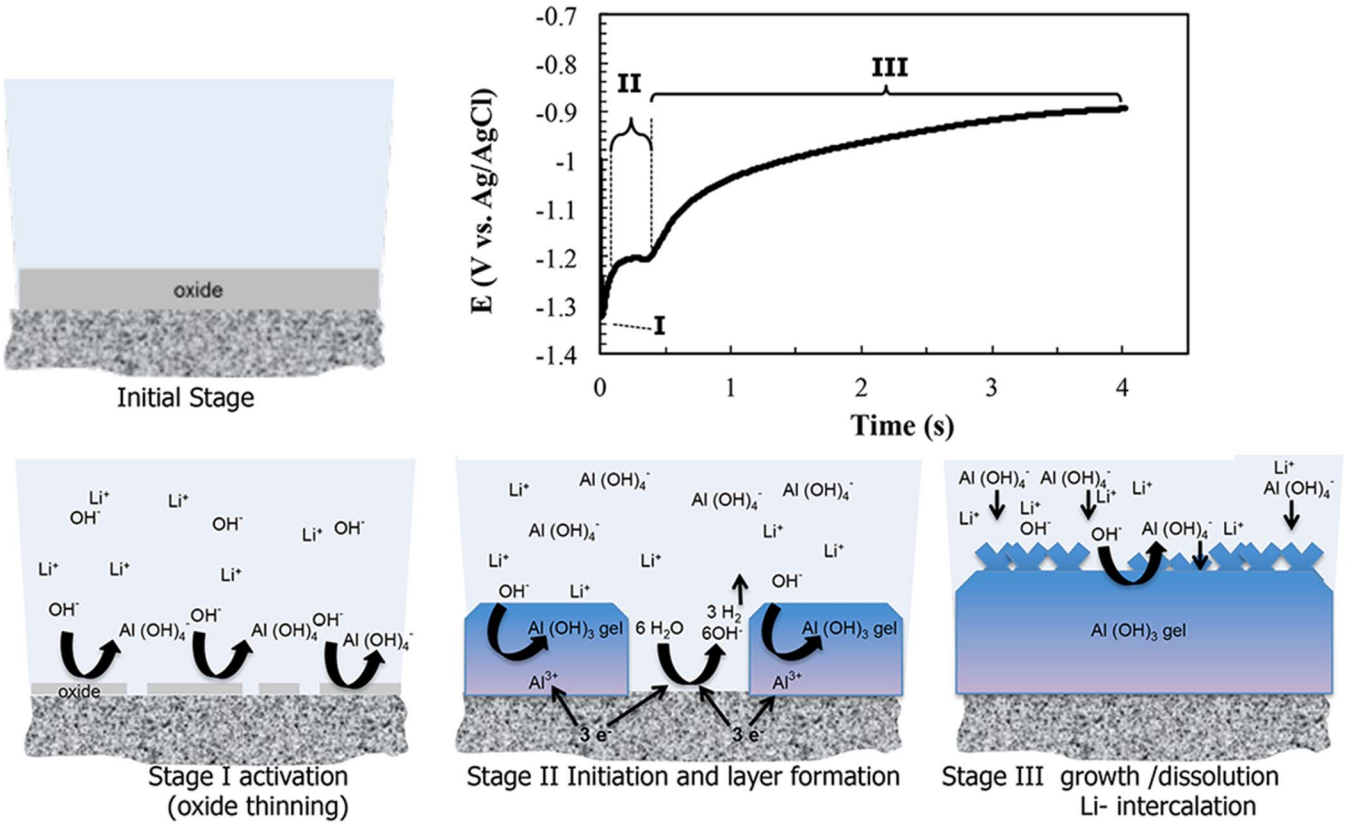

Figure 8. Schematic representation of the formation of the passive layer in relation to the development of the open circuit potential.

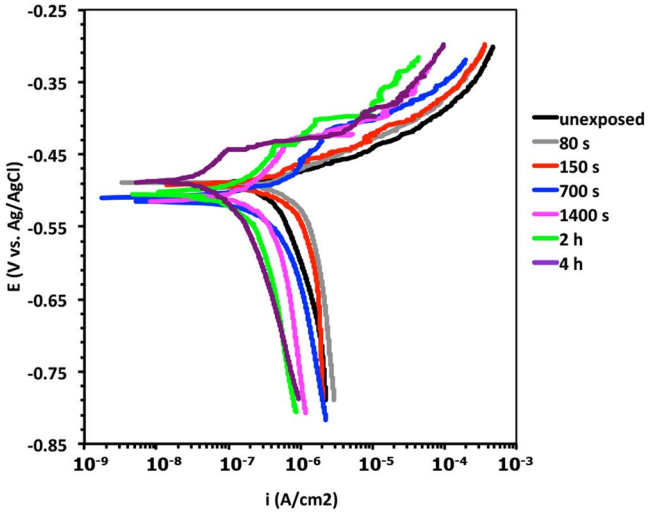

Figure 9. Potentiodynamic polarization curves of the passive layers in 0.05 M NaCl solution as a function of time after exposure to Li_2CO_3-NaCl solution.

samples displayed in Fig. 9. R_{pol} was calculated from the linear slope of the linear region ±20 mV from E_{corr} (Eq. 6). Using this value, i_{corr} was calculated with the Stern-Geary equation (Eq. 7).[35,36]

$$R_P = \left.\frac{\Delta E}{\Delta i}\right|_{E=E_{corr}} \quad [6]$$

In this equation, R_p is the polarization resistance (Ω cm^2), ΔE is change in potential (V) and Δi is change in current (A / cm^2).

$$i_{corr} = \frac{b_a\,|b_c|}{(b_a + |b_c|)2.3R_{pol}} \quad [7]$$

The Stern–Geary equation (Eq. 2) relates the corrosion current to R_p using the anodic (b_a) and cathodic (b_c) Tafel-slopes. From Table III is can be noted that R_{pol} increased as a result of exposure to the Li_2CO_3-NaCl solution from 25 kΩ cm^2, at the initial stage, to around 330 kΩ cm^2 after 4 h and simultaneously the corrosion current density (i_{corr}) decreased over time. This behavior can be attributed to the formation of the passive layer on the anodic and cathodic areas of the aluminum substrate.

EIS measurements.—The electrochemical properties of the layers formed in the Li_2CO_3-NaCl solution were measured by EIS, in a 0.05 M NaCl solution as a function of the exposure time to the Li_2CO_3-NaCl solution, in order to link the electrochemical properties with the different stages of formation of the layer. Fig. 10a shows the development of the Bode impedance modulus as a function of exposure time to the Li_2CO_3-NaCl solution. Compared to the sample prior to exposure (unexposed), the impedance modulus dropped during the first phase until 150 s exposure to the Li_2CO_3-NaCl solution. Following this initial period, the impedance modulus values in the low frequency

Table III. Electrochemical parameters obtained from the potentiodynamic polarization curves displayed in Fig. 9.

	E_{corr} ($V_{(Ag/AgCl)}$)	i_{corr} (A/cm^2)	R_{pol} (kΩ.cm^2)	E_{pit} ($V_{(Ag/AgCl)}$)
initial	−0.50	6.6E-07	24.4	−0.49
80s	−0.50	5.7E-07	29.8	−0.49
150 s	−0.49	3.1E-07	38.8	−0.49
700 s	−0.51	2.1E-07	53.2	−0.43
1400 s	−0.51	1.9E-07	95.8	−0.44
2 h	−0.51	1.5E-07	135.0	−0.45
4 h	−0.48	7.3E-08	332.0	−0.44

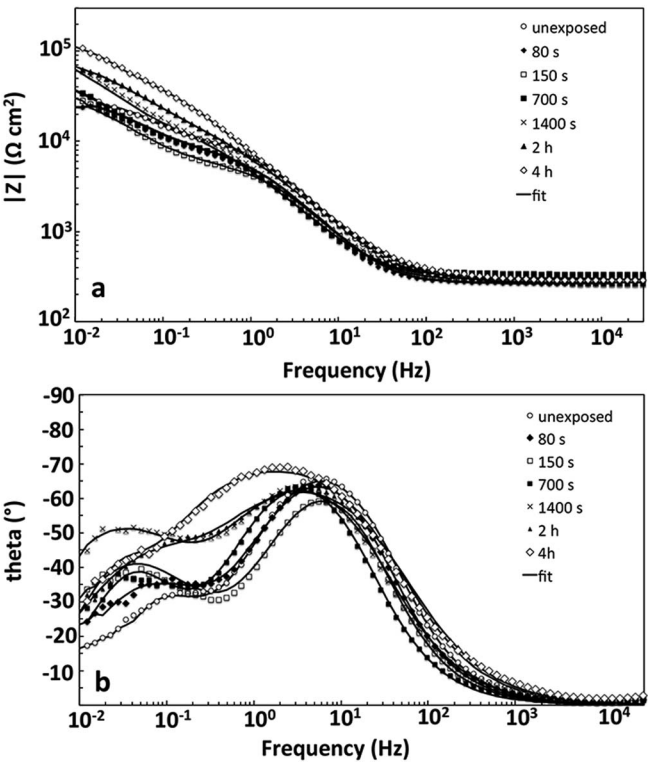

Figure 10. Electrochemical impedance spectra of the AA2024-T3 aluminum alloy in 0.05 M NaCl solution before and after exposure to the Li_2CO_3-NaCl solution (a) impedance modulus and (b) phase angle as a function of exposure time to Li_2CO_3-NaCl solution.

range (10^{-1} – 10^{-2} Hz) started to increase. After 1400s exposure to the Li_2CO_3-NaCl solution the impedance modulus showed increasing values in both the lower and middle frequency range and reached the highest values after 4 h exposure to the Li_2CO_3-NaCl solution. When considering the Bode phase angle plots (Fig. 10b) in general two time-constants can be distinguished, one at the middle frequency range of 10 Hz and one in the low frequency range of 10^{-1} to 10^{-2} Hz. The first time-constant can be attributed to the (oxide) layer and the latter to the electrochemical activity at the aluminum substrate.[37] During the oxide thinning stage (Stage I), 80 and 150 s of exposure to Li_2CO_3-NaCl solution, it can be noticed that the time-constant in the middle frequency range initially decreases and becomes narrower. After 700 s exposure to the Li_2CO_3-NaCl solution, the phase angle plot in the middle frequency starts to broaden. This broadening together with the increase of the impedance modulus in the middle frequency indicates the formation of a layer on the surface of the alloy.[38] This is in agreement with FESEM and Auger results discussed in the previous section.

Based on the physical properties of the layer as observed in the cross-section in Fig. 4, a two time-constant equivalent circuit model (Fig. 11) was selected to fit the EIS measurements and quantitatively describe the electrochemical properties of the layer at the different stages of the formation.[39,40] In this model, R_{sol} is the resistance of the electrolyte. The first time-constant represents the resistance (R_{oxide}) and the capacitance properties (CPE_{oxide}) of the layer that is formed. The second time-constant describes the electrochemical processes (corrosion) at the aluminum substrate in terms of the polarization resistance (R_{pol}) and the double layer capacitance (CPE_{dl}). Constant phase elements (CPE) are used to describe the frequency dependence of elements with a non-ideal capacitive behavior using parameter Q and n.[41] The equivalent capacitance (C) of the respective time-constant was calculated from the resulting R, Q and n values for further comparison and analysis using the equation derived by

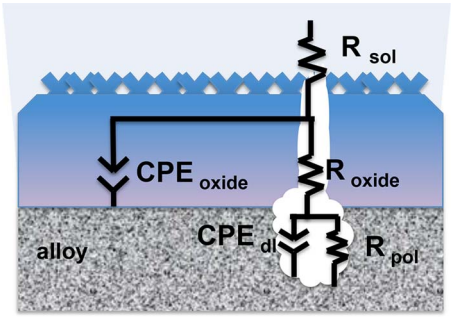

Figure 11. Equivalent electric circuit used to fit EIS spectra for the formed layer from the Li_2CO_3-NaCl solution.

Hirschorn et al. (Eq. 8).[42]

$$C = R^{\frac{(1-n)}{n}} \cdot Q^{\frac{1}{n}} \quad [8]$$

The fitted curves are displayed in Figure 10 and the resistance and capacitance values after the different stages of formation was calculated from at least three measurements. The evolution and scatter of the resistance and capacitance of the oxide/hydroxide layer and the metal/oxide interface as a function of time is shown in Fig. 12. Fig. 12a shows the initial drop of R_{oxide} from 16 to 5 kΩ cm^2 after 80 and 150 s exposure to the Li_2CO_3-NaCl solution followed by a gradual increase over time to a value of about 40 kΩ cm^2 after 4 h exposure to the Li_2CO_3-NaCl solution. On the other hand, the capacitance (C_{oxide}) increased initially from 12 to 42 μF $cm^{2\ after}$ 80 to 150 s and decreases over time when the layer develops over prolonged exposure to the Li_2CO_3-NaCl solution (Fig. 12b). This behavior of R_{oxide} and C_{oxide} aligns with the process of oxide thinning and consequently the formation of the layer. The corrosion activity at the aluminum metal/oxide interface was characterized by the polarization resistance (R_{pol}) and the double layer capacitance (C_{dl}). The evolution of R_{pol} (Fig. 12c) and that of C_{dl} (Fig. 12d) shows a similar behavior of initial decrease of resistance and increasing capacitance followed by increased polarization resistance and decreasing double layer capacitance indicating the formation of a passive layer on the aluminum substrate.

Mechanism of formation and the relation with the electrochemical properties.—The development of electrochemical properties of the layer can be related to the three stages of formation as identified earlier in this paper. Stage I, the oxide thinning phase, is characterized by a fast decrease of the oxide resistance (R_{oxide}) and low polarization resistance values (R_{pol}). Stage II, represents the first indication of the formation of a passive layer. After 700 s exposure to the Li_2CO_3-NaCl solution, R_{oxide} increased by a factor 2 and the potentiodynamic polarization measurements showed decreasing values for the anodic and cathodic current densities and the i_{corr} decreased as well. Stage III is related to the growth and dissolution process of the layer due to the longer exposure to the Li_2CO_3-NaCl solution (1400 s up to 4 h). During this stage the corrosion protective properties of the layer started to increase significantly. At this stage the potentiodynamic polarizations show decreasing values of corrosion current (i_{corr}) and anodic and cathodic current densities. Furthermore, a shift of the pitting potential to more anodic values is observed. This together with the increasing resistance and decreasing capacitance values observed in the EIS measurements demonstrate that the corrosion protective properties of the layer are developing in stage III of the mechanism. At this point the layer is not growing as fast in thickness but the increase in the oxide resistance and decrease of the oxide capacitance suggest

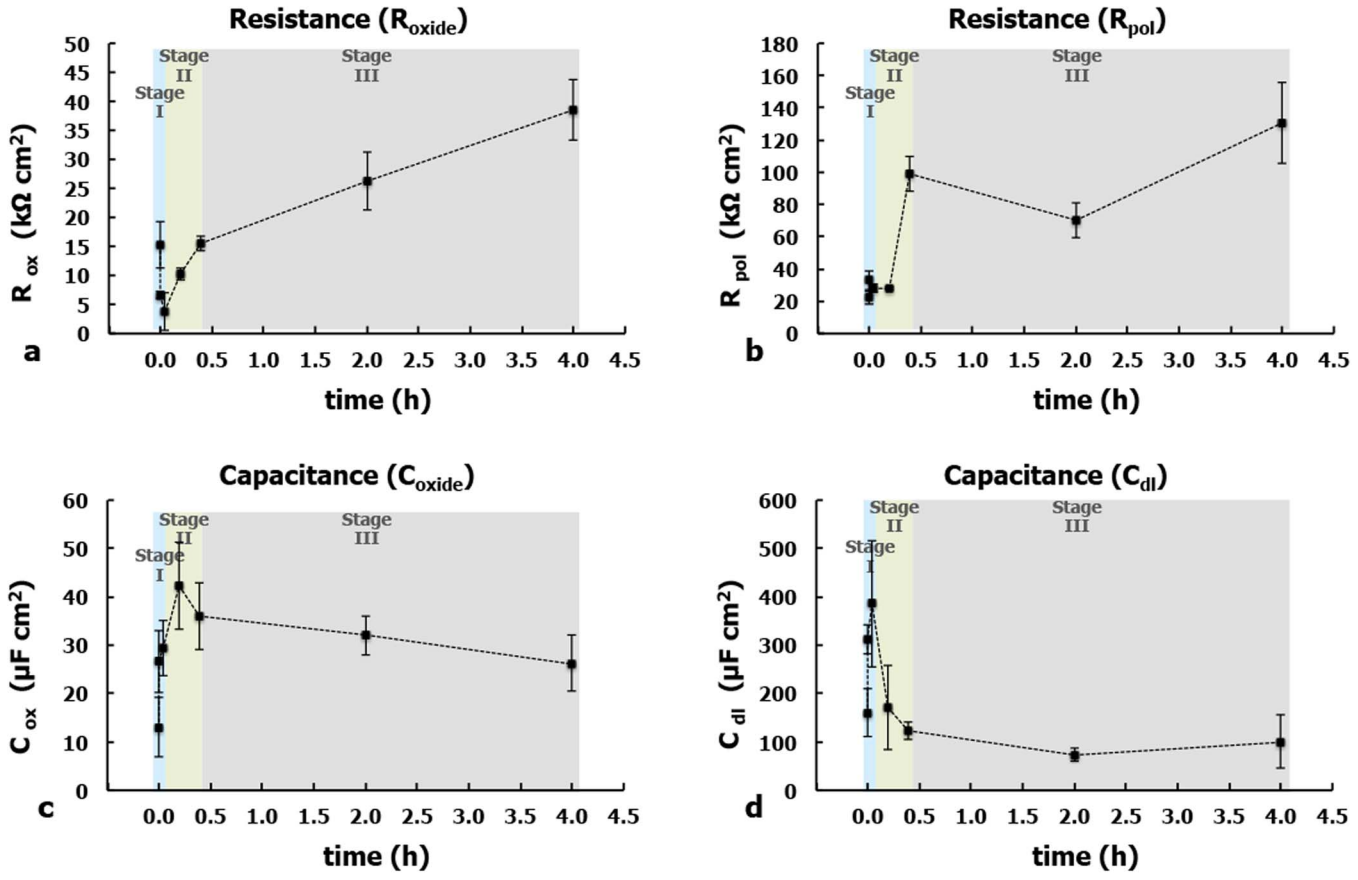

Figure 12. The evolution of the (a) oxide resistance (R_{oxide}), (b) polarization resistance (R_{pol}), (c) oxide capacitance (C_{oxide}), and (d) double layer capacitance (C_{dl}) of the passive layers formed on AA2024-T3 from a Li_2CO_3-NaCl solution in relation to the three stages of formation.

that the layer gains improved passive properties due to a densification process of the amorphous inner layer at the aluminum surface. These observations show that the layer provides fast and effective corrosion inhibition once the surface of the aluminum is covered. These results are in agreement with the observations when lithium-salts are used as leachable corrosion inhibitor in organic coatings.[15]

Conclusions

This work studied the formation mechanism of passive layers on AA2024-T3 from moderate alkaline lithium carbonate solutions in the presence of sodium chloride. A similar layer, as observed in a coating defect when lithium salts are applied as leaching inhibitor, could be generated under conversion conditions in an electrochemical cell. The generated layer consists of an amorphous inner-layer and a crystalline outer-layer. The formation mechanism involves three stages:

- Stage I: Oxide thinning
- Stage II: anodic dissolution and film formation
- Stage III: growth through competitive film formation and dissolution process.

Surface analysis revealed the fast formation of an aluminum hydroxide layer in stage II. During stage III, the layer grows further and the outer aluminum hydroxide layer transforms into a lithium layered double hydroxide (Li-LDH).

Electrochemical characterization confirmed the three phases involved in the formation of the layer and demonstrated that the corrosion protective properties passive properties of the layer can be attributed to the development of the compact inner layer at the aluminum metal/oxide interface during stage III. The results of this study provide an enhanced view and understanding of the active corrosion inhibiting mechanism of organic coatings with lithium salts as leachable inhibitor for the protection of aluminum alloys.

Acknowledgments

The authors acknowledge Marc Raes and Oscar Steenhaut for their assistance with the FE-SEM, XPS and AES. Furthermore, we thank Dr. Yanwen Liu of The University of Manchester for preparing the cross-section of the protective layer in Fig. 1c. This research was carried out under the collaboration agreement between AkzoNobel and Delft University of Technology.

ORCID

Peter Visser https://orcid.org/0000-0002-6388-382X

References

1. J. Gui and T. M. Devine, *Scripta Metallurgica*, **21**, 853 (1987).
2. E. Deltombe and M. Pourbaix, *Corrosion*, **14**, 16 (1958).
3. M. R. Tabrizi, S. B. Lyon, G. E. Thompson, and J. M. Ferguson, *Corrosion Science*, **32**, 733 (1991).
4. S.-I. Pyun and S.-M. Moon, *Journal of Solid State Electrochemistry*, **4**, 267 (2000).
5. J. G. Craig, R. C. Newman, M. R. Jarrett, and N. J. H. Holroyd, *J. Phys. Colloques*, **48**, 825 (1987).
6. R. G. Buchheit, M. D. Bode, and G. E. Stoner, *Corrosion*, **50**, 205 (1994).
7. C. A. Drewien, M. O. Eatough, D. R. Tallant, C. R. Hills, and R. G. Buchheit, *Journal of Material Research*, **11**, 1507 (1996).
8. M. R. S. Castro, J. C. Nogueira, G. P. Thim, and M. A. S. Oliveira, *Thin Solid Films*, **457**, 307 (2004).
9. P. Visser and S. A. Hayes, Pat. WO2010112605-A1, (2010).
10. P. Visser, Y. Liu, H. Terryn, and J. M. C. Mol, *Journal of Coatings Technology and Research*, **13**, 557 (2016).
11. P. Visser, Y. Liu, X. Zhou, T. Hashimoto, G. E. Thompson, S. B. Lyon, L. G. J. van der Ven, A. J. M. C. Mol, and H. A. Terryn, *Faraday Discussions*, **180**, 511 (2015).
12. Y. Liu, P. Visser, X. Zhou, S. B. Lyon, T. Hashimoto, M. Curioni, A. Gholinia, G. E. Thompson, G. Smyth, S. R. Gibbon, D. Graham, J. M. C. Mol, and H. Terryn, *Journal of The Electrochemical Society*, **163**, C45 (2016).
13. Y. Liu, P. Visser, X. Zhou, S. B. Lyon, T. Hashimoto, A. Gholinia, G. E. Thompson, G. Smyth, S. R. Gibbon, D. Graham, J. M. C. Mol, and H. Terryn, *Surface and Interface Analysis*, **48**, 798 (2016).
14. P. Visser, A. Lutz, J. M. C. Mol, and H. Terryn, *Progress in Organic Coatings*, **99**, 80 (2016).
15. P. Visser, M. Meeusen, Y. Gonzalez-Garcia, H. Terryn, and J. M. C. Mol, *Journal of The Electrochemical Society*, **164**, C396 (2017).
16. O. Gharbi, N. Birbilis, and K. Ogle, *Electrochimica Acta*, **243**, 207 (2017).
17. D. Mata, M. Serdechnova, M. Mohedano, C. L. Mendis, S. V. Lamaka, J. Tedim, T. Hack, S. Nixon, and M. L. Zheludkevich, *RSC Advances*, **7**, 35357 (2017).
18. J. D. Gorman, A. E. Hughes, D. Jamieson, and P. J. K. Paterson, *Corrosion Science*, **45**, 1103 (2003).
19. S. T. Abrahami, T. Hauffman, J. M. M. de Kok, J. M. C. Mol, and H. Terryn, *The Journal of Physical Chemistry C*, **119**, 19967 (2015).
20. R. T. Foley, *Corrosion*, **42**, 277 (1986).
21. K. Shimizu, G. M. Brown, K. Kobayashi, G. E. Thompson, and G. C. Wood, *Corrosion Science*, **34**, 1853 (1993).
22. F. Andreatta, A. Turco, I. de Graeve, H. Terryn, J. H. W. de Wit, and L. Fedrizzi, *Surface and Coatings Technology*, **201**, 7668 (2007).
23. G. M. Brown, K. Shimizu, K. Kobayashi, G. E. Thompson, and G. C. Wood, *Corrosion Science*, **34**, 2099 (1993).
24. P. Campestrini, G. Goeminne, H. Terryn, J. Vereecken, and J. H. W. De Wit, *Journal of the Electrochemical Society*, **151**, B59 (2004).
25. R. G. Buchheit, R. P. Grant, P. F. Hlava, B. McKenzie, and G. L. Zender, *Journal of the Electrochemical Society*, **144**, 2621 (1997).
26. M. R. Alexander, G. Beamson, P. Bailey, T. C. Q. Noakes, P. Skeldon, and G. E. Thompson, *Surface and Interface Analysis*, **35**, 649 (2003).
27. A. Nylund and I. Olefjord, *Surface and Interface Analysis*, **21**, 283 (1994).
28. P. A. Schweitzer, *Corrosion and Corrosion Protection Handbook*, M. Dekker (1989).
29. Z. Szklarska-Smialowska, *Corrosion Science*, **41**, 1743 (1999).
30. R. T. Foley and T. H. Nguyen, *Journal of The Electrochemical Society*, **129**, 464 (1982).
31. T. Hurlen and A. T. Haug, *Electrochimica Acta*, **29**, 1133 (1984).
32. G. T. Burstein and R. J. Cinderey, *Corrosion Science*, **33**, 475 (1992).
33. J. Zhang, M. Klasky, and B. C. Letellier, *Journal of Nuclear Materials*, **384**, 175 (2009).
34. G. R. Williams and D. O'Hare, *J Phys Chem B*, **110**, 10619 (2006).
35. M. Stern and A. L. Geary, *Journal of The Electrochemical Society*, **104**, 56 (1957).
36. T. A. Zawodzinski, *Electrochemical Society Interface*, 59 (2009).
37. J. Tedim, M. L. Zheludkevich, A. C. Bastos, A. N. Salak, A. D. Lisenkov, and M. G. S. Ferreira, *Electrochimica Acta*, **117**, 164 (2014).
38. B. Van der Linden, H. Terryn, and J. Vereecken, *Journal of Applied Electrochemistry*, **20**, 798 (1990).
39. G. Yoganandan, J. N. Balaraju, and V. K. W. Grips, *Applied Surface Science*, **258**, 8880 (2012).
40. J. T. Qi, T. Hashimoto, J. R. Walton, X. Zhou, P. Skeldon, and G. E. Thompson, *Surface & Coatings Technology*, **280**, 317 (2015).
41. C. H. Hsu and F. Mansfeld, *Corrosion*, **57**, 747 (2001).
42. B. Hirschorn, M. E. Orazem, B. Tribollet, V. Vivier, I. Frateur, and M. Musiani, *Electrochimica Acta*, **55**, 6218 (2010).